Journal of Materials Chemistry C

Accepted Manuscript

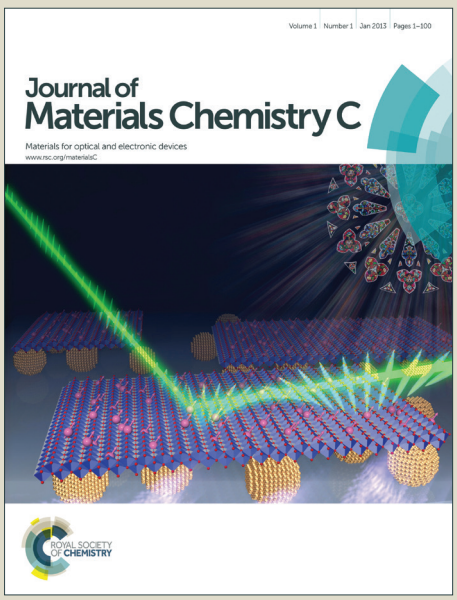

ROYAL SOCIETY OF CHEMISTRY

www.rsc.org/materialsC

Journal of Materials Chemistry

Cite this: DOI: 10.1039/c0xx00000x

www.rsc.org/xxxxxx

PAPER

On the trade-off between processability and opto-electronic properties of single wall carbon nanotube derivatives in thin film heterojunctions

Patrizio Salice,[a] Camillo Sartorio,[b] Alessandro Burlini,[a] Roberto Improta,[c] Bruno Pignataro,*[b] and Enzo Menna*[a]

Received (in XXX, XXX) Xth XXXXXXXXX 20XX, Accepted Xth XXXXXXXXX 20XX
DOI: 10.1039/b000000x

A flow functionalization route has been employed to derivatize single wall carbon nanotubes (SWCNT) by thienylphenyl groups. The SWCNT derivatives in the most soluble fraction have been characterized by thermogravimetric analysis, DLS analysis, DFT calculations, UV-vis-NIR, microRaman and IR spectroscopies to study the degree of functionalization, the concentration of SWCNTs in solution, the dimension of the aggregates in solutions, the density of defects, and the presence of the thienylphenyl groups. Thin film heterojunctions made of SWCNT derivatives and poly(3-hexylthiophene) (P3HT) have been prepared by various methods employing the Langmuir Shaefer technique, spin coating and thermal annealing processes. By comparing the batch and the flow functionalizations a trade-off between solubility, processability and the thin film opto-electronic properties has been found as a result of the degree of functionalization.

Introduction

The use of carbon nanotube (CNT) derivatives brings forth new challenges and opportunities to the materials science community[1, 2] including fields like optoelectronics, photovoltaics, nanolithography, organic electronics, surface coatings, membranes, sensors, biosensors, and so on.[3, 4]

For instance, in the case of bulk heterojunction (BHJ) solar cells, the use of carbon nanotubes instead of [60]- and [70]-fullerene derivatives may lead to improved performance due to the geometric and electronic characteristics of CNTs that are well suited to improve light harvesting, and photo-generation, splitting and diffusion of the excitonic species.[5-9] Indeed, the tubular shape of CNTs provides a large interfacial area and their size is compatible with both the exciton diffusion length (6-20 nm) and the percolation paths (hundreds of nanometers) across the photoactive layer.

Also as to the organic thin film transistors (OTFTs) field, the geometric parameters of CNTs (i.e., chirality index and length) determine their electronic properties, in particular the band gap and the position of their conduction band.[10] The development of scalable techniques aimed at controlling these characteristics has made it possible to obtain semiconducting CNTs with high ambipolar mobilities and high dielectric constants.[11, 12]

As a consequence, the excitons in CNT-based materials have low binding energies and thus a low barrier for exciton dissociation making them promising alternatives to [60]- and [70]-fullerene derivatives for developing heterojunction devices.

Nevertheless, while chemical processes for the preparation of photoactive layers based on conventional small organic molecules and polymers have been largely exploited, the use of carbon nanostructures (CNSs) requires additional developments. Indeed, the strong tendency of CNTs to aggregate hampers their compatibilization in truly nanoscaled composites and may result in phase separation and ultimately in the loss of the foresighted properties associated to their nanometric dimensions.[13] From this scenario it emerges that the first requisite in the design of CNT-based BHJs is to improve the processability of CNTs to tune their interaction with the semiconducting polymer within the photoactive blend, where the key processes of exciton splitting and charge carrier recombination occur.[14] Despite a plethora of CNT-conjugated polymer blends[15, 16] has been reported since the initial findings of Amaratunga[17] and Kymakis,[18-20] BHJ solar cells based on these blends often fail to afford satisfying photo-conversion efficiencies.[21, 22] Indeed, suitable processing techniques and affordable chemical strategies need to be further developed to optimize the blend morphology and to improve the electronic interaction between the polymer and the CNTs.[23] Nicholas group has been amongst the first to focus on the development of functionalization processes to optimize the interface between conductive polymers and CNTs.[24] The authors reported the non-covalent functionalization of (6,5) single-walled carbon nanotubes (SWCNTs) with a monolayer of poly-(3-hexylthiophene) (P3HT) to obtain nanometric heterojunctions with both excellent alignment and ultrafast charge transfer rates. While this strategy is effective in lab scale quantities, covalent functionalization processes which form stable bonds at the surface of CNTs are more advisable to prepare functionalized carbon nanostructures with enhanced solubility and processability on a larger scale.[25, 26] Indeed, the chemistry of CNTs is now rich with a variety of reactions, including oxidation with strong oxidants,[27, 28] addition of carbenes,[29] addition of organolithium,[30] 1,3-dipolar cycloaddition[31] and addition of diazonium salts.[32, 33] The last class of reactions is particularly indicated to modify surface properties

(such as solubility, adhesion and biocompatibility) of carbon nanostructures.[34, 35] In the case of CNTs, we have demonstrated that the combined use of suitable dispersing solvents, (e.g., 1-cyclohexyl-2-pyrrolidone, CHP)[36, 37] and of flow reactors[26, 38] enables process intensification while preserving a tight control on the reaction conditions, and thus on the properties of functionalized CNTs, including solubility, aggregation size and functionalization degree (FD).

Since the interaction of functionalized CNTs with the surrounding medium is determined by the amount and by the distribution of functional groups on their surface,[39, 40] we devised an affordable synthetic strategy in flow conditions that provides high degree of control on the addition of the reactive aryl diazonium salts to CNTs and ultimately on the properties of the resulting products.[41] These results find application in the present work, where we report on the preparation of photoactive heterojunction devices, as in the case of a blend of P3HT as p-type electron donor semiconducting polymer and derivatized SWCNTs as n-type electron acceptor semiconducting nanostructures. In particular, SWCNTs have been functionalised with 4-(thien-2-yl)phenyl (**PhTh**) moieties, and the interaction of the **SWCNT-PhTh** derivatives with P3HT in thin film blends has been investigated.

Experimental

Materials and methods

All the reagents and solvents were purchased from Sigma-Aldrich and were used as received if not otherwise specified. SWCNTs were purchased from CNI (lot # P2150) and were used as received. CHP was distilled at 104°C and 0.05 mbar prior to use. Dihydroxy-thien-2-ylborane[42] and tert-butyl(4-iodophenyl)carbamate[43] were synthesised according to literature procedures. Melting points of compounds were measured with a Q20 DSC (TA Instruments). ^{1}H and ^{13}C-NMR spectra were collected using an Avance 300 MHz NMR spectrometer (Bruker) and $CDCl_3$ as a solvent. Multiplicity is given as follows: s = singlet, d = doublet, dd = doublet of doublets, m = multiplet, br = broad peak. Centrifugations were performed on a MR23i Jouan ultracentrifuge equipped with a SWM 180.5 swinging bucket rotor (Thermo electron corporation) at 3000 rpm for 10 minutes. Absorption spectra in air-equilibrated solvents were registered with a Varian Cary 5000 spectrophotometer, at room temperature, between 280 and 1400 nm, data interval = 0.5 nm, scan rate = 300 nm/min, SBW = 2 nm. Dispersions of SWCNTs were achieved using the Sonicator 3000 (Misonix) with the following pulse parameters: time on = 3 sec, time off = 3 sec, power level = 2 (4-6 watt) for 30 minutes. Dynamic light scattering (DLS) measurements of nanotube samples dispersed in air-equilibrated chlorobenzene were performed with a Zetasizer Nano S (Malvern Instruments) at 20 °C setting 20 runs of 10 seconds for each measurement. Raman spectra of CNSs, drop-casted on pre-cleaned glass micro slides (Corning) and annealed at 110°C, were recorded with an Invia Renishaw Raman microspectrometer (50× objective) using the 633 nm line of a He–Ne laser at room temperature with a low laser power. IR spectra of the samples were collected on a Thermo Scientific Nicolet 5700 FT-IR spectrophotometer equipped with an attenuated total reflection module (Smart Omni sampler, Ge crystal). Spectra were measured at a resolution of 4 cm^{-1}. Thermogravimetric analyses (TGA) of CNS samples, precipitated by adding methanol and dried at 80 °C at 0.2 mbar for 4 h, were carried out with a Q5000IR TGA (TA Instruments) under nitrogen by an isotherm at 100 °C for 10 minutes followed by heating at 10 °C/min rate till 900 °C.

The flow reactor used for the functionalization of carbon nanotubes has been previously described[38] and it consisted of a 400 cm segment of polytetrafluoroethylene (PTFE) tubing (i.d. = 800 μm) for a total volume of 2.0 mL. The reagent stream was injected into the reactor heated at 80˚C by an HPLC pump (Model KP-12-01S, Flom, Tokyo, Japan) providing a flow rate of 8.0 mL/h, corresponding to a residence time of 15 minutes. The inlet of the reactor was properly fitted with a three-way valve to control the loading of the CNT suspension into the PTFE injection loop (O.D. = 2.0 mm, volume = 11 ml) and the outlet was fitted with a mechanical back-pressure regulator (S series Metering Valve, Swagelok).

Synthesis

***Tert*-butyl (4-(thiophen-2-yl)phenyl)carbamate (1).** The reaction was carried out under nitrogen atmosphere. $Pd(PPh_3)_2Cl_2$ (160 mg, 0.23 mmol) and an aqueous solution of Na_2CO_3 (1 M, 9 mmol) were added to a solution of dihydroxy-thien-2-ylborane (600 mg, 4.7 mmol) and tert-butyl(4-iodophenyl)carbamate (0.77 g, 2.9 mmol) in THF (40 mL). The resulting mixture was heated at reflux. The reaction was monitored by thin layer chromatography (TPC) on silica gel (eluent: ETP/ Et_2O 4:1, R_f = 0.35). After 180 minutes, the reaction was quenched with a saturated aqueous solution of NH_4Cl (50 mL) and washed with AcOEt (3 x 50 mL). The organic phase was dried over Na_2SO_4 and the solvent was removed at reduced pressure obtaining a yellow solid which was purified by column chromatography on silica gel (eluent: ETP/ Et_2O 4:1, R_f = 0.35). The desired product was obtained as yellow powder (360 mg). 56% yield (0.36 g). m.p. = 192-194 °C; ^{1}H-NMR (200 MHz, DMSO-d_6): δ (ppm) 10.01 (br, 1H), 7.60 (m, 4H), 7.47 (dd, 1H), 7.41 (dd, 1H), 7.10 (dd, 1H), 2.02 (s, 3H). ^{13}C-NMR (50 MHz, DMSO-d_6): δ (ppm) 168.3, 143.3, 1338.8, 129.2, 129.0, 126.5, 125.5, 123.5, 120.0, 24.0. Anal. Calcd for $C_{15}H_{17}NO_2S$: C, 65.43; H, 6.22; N, 5.09; S, 11.64. Found: C, 65.27; H, 6.45; N, 4.89; S, 11.33.

4-Thien-2-ylaniline (2). A solution of **1** (170 mg, 0.62 mmol) in CH_2Cl_2 (5 mL) was treated with trifluoroacetic acid (TFA, 57 μL, 0.74 mmol). After 45 minutes, the reaction was quenched with a 1 M aqueous solution of NaOH (100 mL) and washed with AcOEt (3 x 50 mL). The organic phase was dried over Na_2SO_4 and the solvent was removed at reduced pressure obtaining the desired product as yellow powder (107 mg). 99% yield. m.p. = 72-74 °C; ^{1}H-NMR (200 MHz, DMSO-d_6): δ (ppm) 7.25 (m, 3H), 7.13 (dd, 1H), 6.96 (dd, 1H), 5.21 (br, 1H). ^{13}C-NMR (50 MHz, DMSO-d_6): δ (ppm) 149.2, 145.6, 128.8, 127.1, 123.3, 122.3, 121.1, 114.7.

Batch functionalization of CNTs (SWCNT-PhTh)

As a reference, SWCNTs were functionalized in a batch process.[32, 44-46] Briefly, freshly prepared 4-thien-2-ylaniline (**2**) (130 mg, 0.74 mmol) and isopentylnitrite (100 μL, 0.74 mmol) were added to a dispersion of SWCNTs (9.0 mg, 0.75 mmol) in CHP (5 mL) pre-heated at 80 °C. After 4 h, the reaction mixture was quenched in

methanol (100 mL) and then centrifuged at 3000 rpm for 3 minutes, the supernatant was removed and the black residue was washed with methanol (5 x 7 mL). The residual carbon material was dried under vacuum (0.2 mbar) at 80 °C for 4 h, weighted and characterised.

Flow functionalization of CNTs (SWCNT-PhTh)

A solution of SWCNTs (8.9 mg, 0.74 mmol C) in CHP with concentration 2 mg/mL was sonicated for 1 h. Then the aniline **2** (130 mg, 0.74 mmol) and isopentylnitrite (100 µL, 0.74 mmol) were added to the dispersion of SWCNTs and immediately loaded in the injection loop of the flow reactor. The reaction mixture collected from the reactor was quenched in methanol (100 mL) and then centrifuged at 3000 rpm for 3 minutes. The supernatant was removed and the black residue was washed with methanol (5 x 7 mL). The residual carbon material was dried under vacuum (0.2 mbar) at 80 °C for 4h, weighted and characterised.

Characterization of functionalized CNTs

Aliquots of the soluble **SWCNT-PhTh** derivative were extracted by means of sonication/centrifugation cycles. For each washing cycle, 7.0 mL of chlorobenzene were added to the CNT material obtained after the functionalization processes. The concentration of each solution of SWCNT-PhTh were calculated contextually to the TGA measurements. Briefly, 500 µL of each solution was drop cast and annealed at 120°C on a platinum crucible for TGA analysis. The weight measured at the beginning of the TGA analysis was used to calculate the concentration of SWCNT-PhTh in solution. The first extract for each reaction was subjected to UV-vis-NIR, Raman and ATR-IR spectroscopies, DLS and TGA.

Preparation of thin-film heterojunctions

Multilayer planar heterojunctions (MHJ) were realized by depositing alternated thin layers of poly(3-hexylthiophene-2,5-diyl) (P3HT regioregular, electronic grade, 99.995%, average Mn 15000–45000, Aldrich) and SWCNTs by Langmuir-Schafer technique (LS). In particular, Langmuir films were deposited using a KSV Minitrough apparatus. Ultrapure Millipore filtered water with resistivity greater than 18.2 MΩ·cm was used as the subphase at a temperature of 25 °C. A solution of 0.1 mg/mL of P3HT in chloroform (Aldrich, 99.9%) was randomly spread over the aqueous surface by a microsyringe. After solvent evaporation (about 10 min) the floating films were linearly compressed by means of two mobile barriers at a rate of 5 mm·min^{-1}. The ultrathin films, at a 20 mN·m^{-1} surface pressure, were transferred layer by layer on the indium tin oxide coated poly(ethyleneterephthalate) (ITO/PET) square substrates (about 1 cm^2). To obtain a BHJ, the MHJ architectures have been heated at a temperature close to the glass transition temperature of P3HT. This thermal annealing allows increasing the molecular interdiffusion within the bilayer system and induces the formation of an interpenetrating system typical of a BHJ. To realize spin-coated BHJ, P3HT was dissolved in the SWCNTs solutions. The resulting P3HT:SWCNTs mixtures were spin-coated onto ITO/PET substrates at 1500 rpm for 30 seconds.

Characterization of thin films

Fluorescence spectra were recorded using a Fluoromax-4 (HORIBA Jobin Ivon, Edison, USA) spectrofluorimeter equipped with a 150 W xenon arc lamp as excitation source. Spectroscopic analyses were performed directly on freshly prepared thin films of both pure P3HT and P3HT/SWCNTs heterojunctions. Heterojunction quenching data were normalized to the fluorescence of P3HT thin films.

Computational details

Our computations are based on Density Functional Theory (DFT) and its time-dependent extension (TD-DFT) for the study of excited states. We used the CAM-B3LYP functional (that has already been successfully applied to the study of dithiophene),[47] while solvent effect have been included by the Polarizable Continuum Model (PCM).[48] All the calculations have been performed by Gaussian09 program.[49]

Fluorescence quenching experiments

In a typical experiment, the intensity of the fluorescence emission of a fluorophore solution is measured after each addition of a stable dispersion of CNTs. In our case, we added consecutive aliquots of a solution of **SWCNT-PhTh**, both flow- and batch-functionalised, to a solution of P3HT in chlorobenzene and we measured the emission at 575 nm after each addition. The intensities were then corrected both for the increasing dilution and for the inner filter effect due to the absorption of **SWCNT-PhTh** . Indeed, the absorption of CNTs throughout the visible spectrum results in the reabsorption of the light emitted at 575 nm by P3HT and could significantly affect these measurements (See Fig. 2).

Results and discussion

In Scheme 1, we report the synthesis of the 4-(thien-2-yl)aniline (**2**) used for the preparation of **SWCNT-PhTh**.

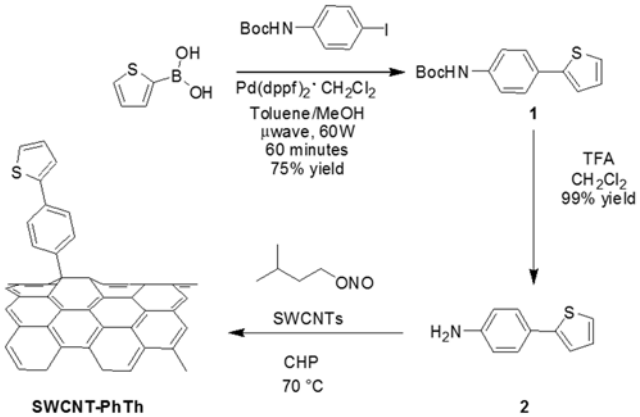

Scheme 1 Functionalization of SWCNTs via addition of the diazonium salt of 4-(thien-2-yl)aniline (**2**).

The thienyl group was previously proposed as a motif of interaction between CNTs and polythiophenes in the photoactive layer of BHJs.[50, 51] The derivatization of an aniline with a thienyl group was achieved by Suzuki-Miyaura coupling between Boc-protected 4-iodoaniline and 2-thiophenboronic acid to yield the carbamate **1** followed by deprotection of the Boc group with trifluoroacetic acid. The resulting 4-(thien-2-yl)aniline **2** was reacted with isopentylnitrite in CHP to generate in situ the

diazonium salt used for the derivatization of CNTs. We chose to derivatize SWNCTs produced by the HiPco process due to their prevailing semiconducting behaviour which makes them suitable electron acceptors in BHJs.[52, 53] For the functionalization of SWCNTs, we initially followed reported approaches based on reactions in a flask at 80 °C for 4 h.[54] In these conditions, we expected to obtain highly soluble and extensively functionalized CNTs. In fact, we have recently observed that an extensive functionalization by addition of diazonium salts to MWCNTs in batch conditions results in the growth of aryl layers on the surface of CNTs which further enhance their solubility in common organic solvents (e.g., ethanol).[41] Nevertheless, a covalent functionalization inducing a large increase in the density of C sp^3 defects in the C sp^2 backbone leads to the deterioration of the electronic properties of the CNTs.[29] As a consequence, a tight control on the reaction conditions is necessary to reach a trade-off between solubility of the functionalized CNTs and the resulting density of sp^3 defects. Considering that flow reactors offer higher productivity, increased safety and tighter control on the reaction parameters with respect to traditional batch processes, we have introduced the functionalization of CNTs in flow as a valuable alternative to traditional batch processes.[26, 38] Under this perspective, we functionalized HiPco SWCNTs by addition of the diazonium salt of the aniline **2** also in a flow reactor, by setting a flow rate of 8.0 mL/h and a temperature of 80 °C. Then, we relied on a robust protocol to purify, characterize and compare the products of the functionalization in batch and in flow conditions.[38] Briefly, the functionalized carbonaceous materials obtained at the end of the addition reaction were quenched in methanol, collected by centrifugation and washed with methanol to remove the solvent (CHP), byproducts and excess reactants. At this stage of the derivatization process, the functionalised material consists of a mixture of SWCNTs with different FD and solubility. Being interested in the preparation of solution-processable SWCNT/P3HT blends, we isolated soluble fractions of **SWCNT-PhTh** derivative by extraction with chlorobenzene (in which P3HT is soluble). Practically the soluble derivatives were collected through dispersion of the CNT material by pulsed sonication in chlorobenzene, precipitation of the less soluble aggregates by centrifugation and collection of the supernatant. These steps were repeated five times on each sample thus obtaining five fractions with decreasing concentrations for both batch and flow-processed **SWCNT-PhTh** (see Fig. 1).

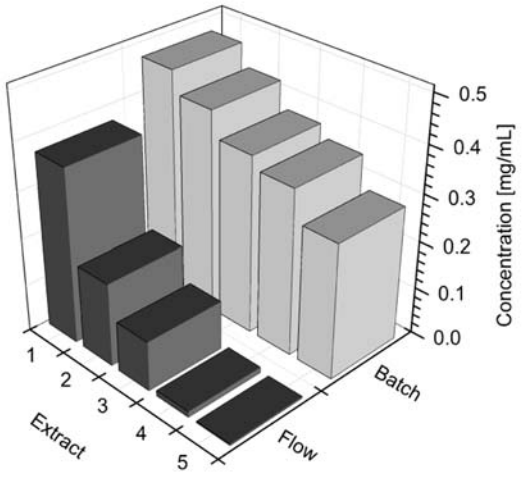

Fig. 1 Solubility profile in chlorobenzene for **SWCNT-PhTh** derivatised in flow (dark grey) and in batch (light grey).

The comparison between the solubility profiles shows that both functionalization processes led to a significant increase in the maximum solubility (0.47 mg/mL and 0.37 mg/mL for **SWCNT-PhTh** synthesised in batch and in flow, respectively) in chlorobenzene compared to pristine HiPco SWCNTs (0.017 mg/mL). Nevertheless, the two solubility profiles are remarkably different. The sample functionalized in batch has a high mean solubility and is completely extracted within five fractions. On the other hand, the rapidly decreasing concentration profile in the case of flow synthesis indicates that only a fraction of the starting material has gained enough solubility and thus is extracted with chlorobenzene within the five fractions (4.7 mg over 8.9 mg of starting material)

The most soluble fractions for **SWCNT-PhTh** functionalized in batch and in flow conditions were further characterized by UV-vis-NIR, Raman, and ATR-IR spectroscopies, TGA, and DLS.

Using DLS we estimated the dimension of the soluble aggregates of CNTs in chlorobenzene. Both samples present a distribution of particles with an average solvodynamic diameter up to 100 nm, consistently with their proposed use as functional nanofiller in BHJs. In particular, **SWCNT-PhTh** obtained in batch and that obtained in flow form bundles with an average diameter of 50 and 100 nm respectively (see Supporting Info, page S8, figure S7).

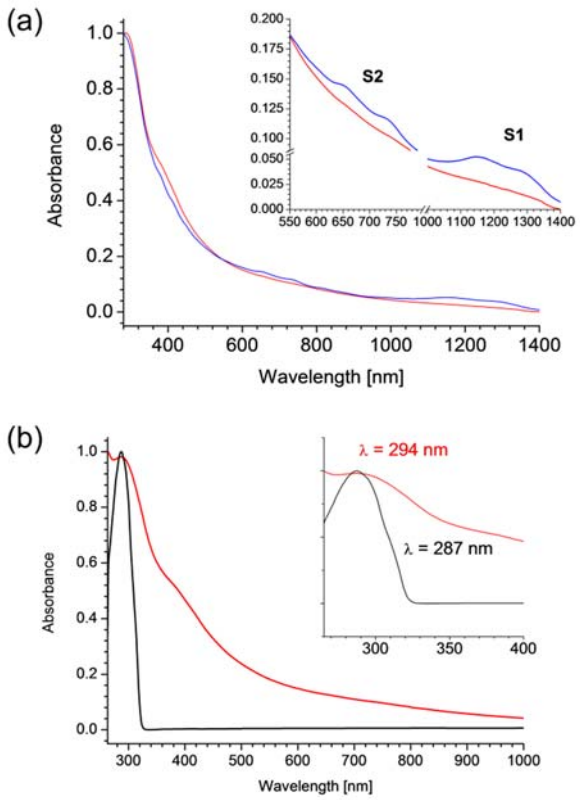

Fig. 2 Comparison between the UV-vis-NIR spectra in chlorobenzene of (a) **SWCNT-PhTh** synthesized in batch (red) and in flow (blue) conditions. The inset highlights the spectral regions of Van Hove singularities (S2 and S1). (b) **SWCNT-PhTh** obtained in batch (red) and 2-(*p*-tolyl)thiophene (black). The inset highlights the absorbance bands due to thienylphenyl residues.

The UV-vis-NIR absorption spectra of the most soluble extracts of **SWCNT-PhTh** in chlorobenzene are reported in Fig. 2a. The inset highlights the lack of the absorbance bands due to electronic transitions between Van Hove singularities (S2 and S1) in the batch sample. Indeed, the nanotubes functionalized in batch are characterized by the typical SWCNT plasmonic absorption centred below 260 nm together with a band around 294 nm. Such band is not far from the maximum absorption wavelength of the model compound 2-(*p*-tolyl)thiophene, as reported in the inset in Fig. 2b, and thus it might be ascribed to the functional moiety grafted to the nanotube backbone. We resorted to first principle TD-DFT calculations in solution to confirm that the functionalization of SWCNTs may result in a bathochromic shift of 0.10 eV (7 nm) of the absorption band of the **PhTh** moiety. In table 1, the vertical excitation energies (ν_A) of 2-(*p*-tolyl)thiophene computed in an apolar environment are compared with those obtained on the system **II**, the minimal model for a **PhTh** bonded to the SCWNT surface (see Fig. 3),where the methyl group bears three ethylene substituents (mimicking the interaction with the nanotube). Our calculations predict that the interaction with the π system of the ethylene groups leads to a weak red-shift of ν_A, supporting our assignment of the feature at 294 nm in **SWCNT-PhTh** absorption spectra to the PhTh moiety. The lowest energy absorption band is due to a strong ππ* transition, that can be described as deriving from a HOMO→LUMO excitation.

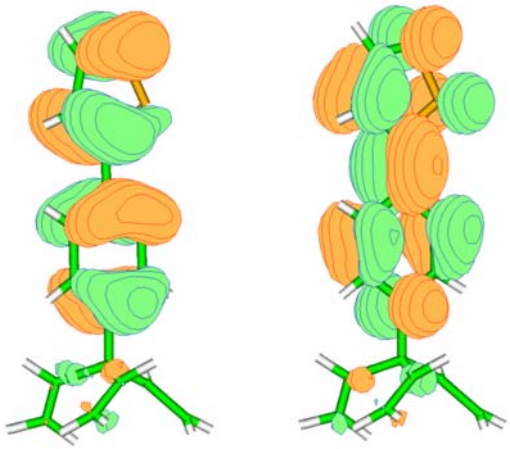

Fig. 3 Schematic description of the HOMO (left) and the LUMO (right) of the model system **II**

Inspection of the frontier orbitals of **II** shows that the π Molecular Orbitals (MO) of the three ethylene substituents on the terminal methyl have a small but not negligible contribution both to the HOMO and the LUMO. The interaction, antibonding, i.e. leading to a destabilization of the MO, is larger for the LUMO, explaining the small red-shift of the HOMO ➔ LUMO transition.

The same trend is found for both the non-planar absolute minima and for the planar saddle point that has been suggested to be the best reference structure for computing the oligothiophene absorption spectra.[47] Our computed ν_A are in very good quantitative agreement with the experiments, especially when considering that, in a strongly related compound as dithiophene, vibrational effects lead to a 0.2~0.3 eV red-shift of the computed band maximum with respect to ν_A.[47]

Table 1: Computed Vertical Excitation Energies (in eV, values in nm reported in italics) of 2-(*p*-tolyl)thiophene and system **II** in chloroform, computed at the PCM/TD-CAMB3LYP/6-311+G(2d,2p)//CAMB3LYP/6-31G(d) level. Oscillator strengths in parentheses

	2-(*p*-tolyl)thiophene	II
Planar saddle point	4.29 (0.60) *288.7*	4.27 (0.73) *290.3*
Non-planar minimum	4.52 (0.58) *274.5*	4.48 (0.73) *277.0*

These findings suggest that the surface of SWCNTs functionalized in batch is heavily covered with 4-(thien-2-yl)phenyl functionalities. On the other hand, the spectrum of flow-synthesised **SWCNT-PhTh** shows both the plasmon contribution and the absorption features due to the Van Hove singularities of semiconducting SWCNTs between 550 and 800 nm (S2) and between 1000 and 1400 nm (S1), but lacks the band at 294 nm ascribed to the **PhTh** functionality. These observations are consistent with a lower FD compared to the sample processed in batch conditions, allowing to retain, at least in part, the semiconducting characteristics of the pristine HiPco nanotubes upon flow functionalization.

Further evidence comes from the comparison of the Raman spectra of the samples from batch and flow functionalization reported in Figure 4a.

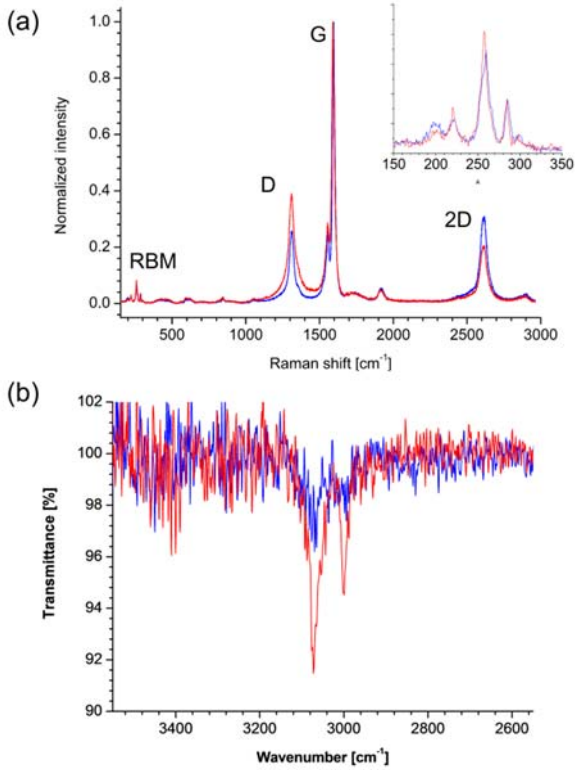

Fig. 4 Comparison between **SWCNT-PhTh** derivatised in batch (red) and in flow (blue) conditions: (a) Raman (the inset highlights the radial breathing modes) and (b) IR spectra.

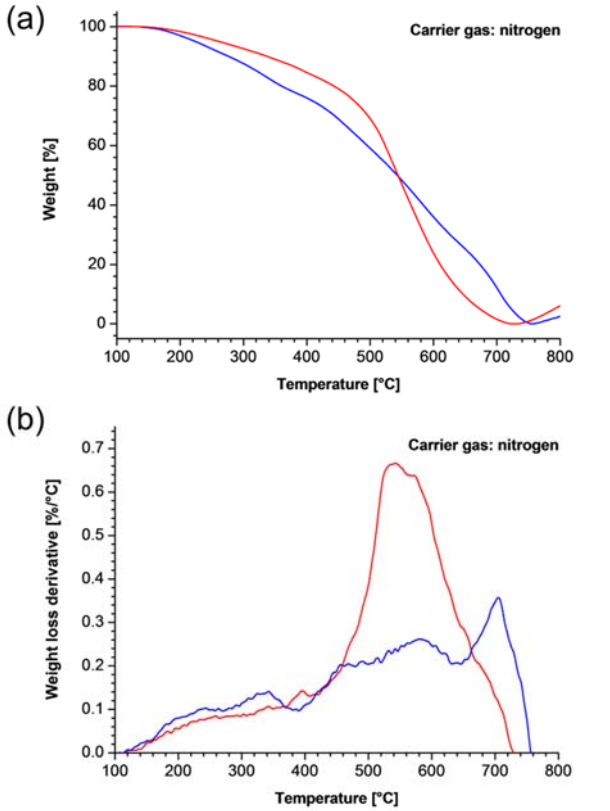

Fig. 5 Comparison between (a) thermograms of **SWCNT-PhTh** derivatised in batch (red) and in flow (blue) (carrier gas: nitrogen; heating rate: 10 °C/min) and (b) between the corresponding weight loss derivatives.

Both functionalization processes resulted in an increase of the ratio between the intensity of the D band at about 1300 cm^{-1} and that of the G band centred at about 1650 cm^{-1} (D/G ratio) with respect to the starting material (see Supporting Info, page S9, figure S8). This behaviour is in agreement with the expected reduction of the size of sp^2 domains, due to the conversion of sp^2 carbons to sp^3 carbons upon reaction with aryl diazonium salts. Noticeably, the increase in the D/G ratio is more pronounced for the material processed in batch conditions indicating that it has endured a more extensive modification of the sp^2 backbone than the material processed in flow conditions. Moreover, the dramatic reduction of the intensity of the 2D band at 2650 cm^{-1} in the sample processed in batch reveals strong perturbation in the electronic and phononic structure of CNTs.[56, 57] Finally, the radial breathing modes are not subjected to particular variations for both samples suggesting that the 1D-form factor of SWCNTs is maintained. Complementary to Raman spectroscopy, which is particularly sensitive to the CNT backbone, IR spectroscopy gives information on the functional groups attached to their surface. The comparison between the IR spectra of **SWCNT-PhTh** derivatised in batch and in flow is reported in Figure 4b. In both cases the C-H stretching modes of aryl groups (at ~3000 and ~3100 cm^{-1}) are recognizable but the intensity of the peaks is low as expected for sparse functional groups grafted to the CNT surface. The qualitative evaluation provided so far arguably implies that the sample prepared in batch is more soluble and has a higher defect density with respect to the sample derivatised in flow conditions.

Since pristine SWCNTs are thermally stable up to 700 °C (Supporting Info, page S6, figure S5), it is normally assumed that organic groups attached to the CNT surface decompose at a lower temperature than the carbon backbone. This allows to obtain a quantitative estimate of the FD by thermogravimetric analysis.[28] Nevertheless, the thermal analysis of the two samples reported in the thermograms and in the corresponding weight loss derivatives in Figure 5 suggest a more complex behaviour. The sample prepared in batch is characterized by two peaks in the weight loss derivative graph corresponding to a thermal decomposition below 400 °C followed by a second one centred at 550 °C. As we previously reported,[41] a fast and premature pyrolysis of CNTs derivatised via addition of aryl diazonium salts is observed when the functionalization is very intensive, so that nanotubes are almost completely degraded at 700 °C. In this case the weight loss ascribed to the organic fraction and that of the carbon nanostructure are hardly discriminated, thus hampering a reliable calculation of the degree of functionalization. Interestingly, the weight loss derivative for **SWCNT-PhTh** prepared in flow conditions shows an additional peak centred at 700 °C. This may suggest that functionalization in batch conditions has reduced the thermal stability of CNTs more markedly than flow-functionalization.

So far we have provided evidence that flow-functionalization affords products with good solubility and lower FD with respect to batch processing. Then, we used fluorescence spectroscopy to prove that the differences in the functionalization result in different interaction with P3HT. We started from the consideration that a

charge-transfer interaction between a fluorophore and a CNT should provide a non-radiative deactivation pathway for the first excited state of the fluorophore, thus quenching its fluorescence. Indeed, evidence of the interactions between porphyrins, phthalocyanines and polycyclic aromatic hydrocarbons with CNTs was obtained with a series of steady state and time resolved spectroscopic methods.[58] The reported results confirm that charge separation evolves from the excited state of the fluorophore to the SWCNT upon photoexcitation. This phenomenon is quantifiable by the Stern-Volmer equations from a fluorescence quenching experiment.

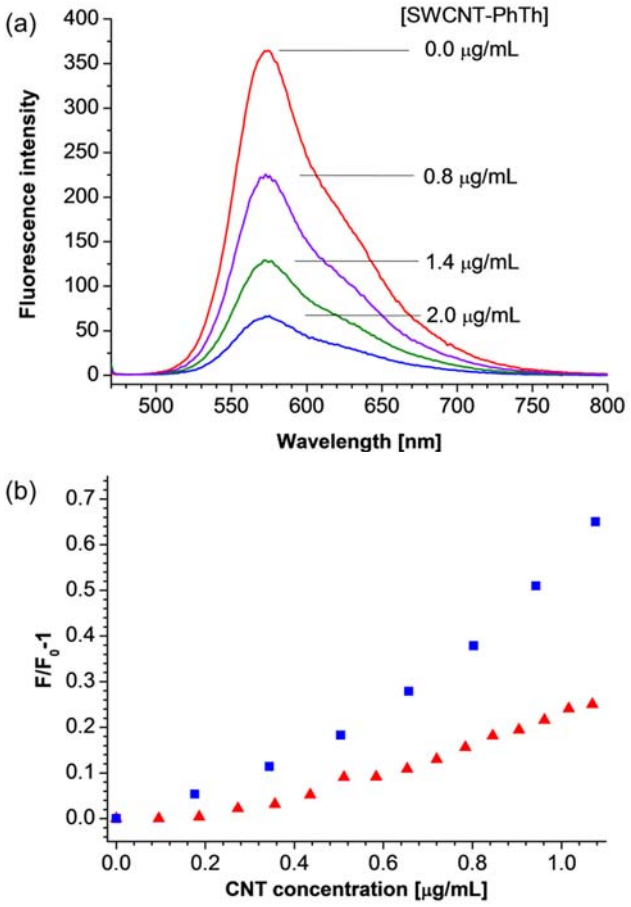

Fig. 6 (a) Emission spectra of P3HT in chlorobenzene with increasing concentrations of **SWCNT-PhTh** functionalized in flow. (b) Stern-Volmer plot of the quenching of P3HT by **SWCNT-PhTh** functionalized in flow (blue squares) and in batch (red triangles).

As reported in Fig. 6, the addition of **SWCNT-PhTh** functionalized in flow to a solution of P3HT resulted indeed in the reduction of the fluorescence emission intensity. Once reported in the Stern-Volmer plot as a function of **SWCNT-PhTh** concentration (i.e., the quencher), we obtained an upward curve for both the sample functionalized in flow and in batch conditions. This behaviour indicates that two concurrent mechanisms are possible: a dynamic quenching due to collisions between excited P3HT and **SWCNT-PhTh** and a static quenching resulting from the formation of a ground state complex between P3HT and **SWCNT-PhTh**. These results are consistent with the reported CNT-induced fluorescence quenching of Rhodamine B.[59] In that case a consistent ground state deactivation was found.

Interestingly, fluorescence quenching of P3HT by **SWCNT-PhTh** functionalized in flow conditions is more pronounced than for those functionalized in batch conditions.

On the basis of the results obtained in solution we replicated the fluorescence quenching experiments in a solid state photoactive blend composed of P3HT and **SWNT-PhTh**. Indeed, the performance of electronic devices is very sensitive to the nanoscale architecture of the active layer, since key properties like for instance the photovoltaic behaviour or the field effect mobility in ambipolar devices are strongly related to the structural order. In general, ensuring a good mixing of the two components (P3HT and **SWNT-PhTh**) is not a sufficient condition to obtain a performing active layer. For instance, in organic photovoltaics, it's crucial that P3HT and SWCNTs create a bicontinuous system with domains that have a size comparable to the length scale of exciton diffusion (i.e., ~5-20 nm). At the same time, the domains must ensure extended percolation channels for the charge carriers. Among the possible processes to prepare thin films with high control on morphology and structure, we exploit the Langmuir-Schaefer technique for the realization of a multi-planar heterojunction (MHJ) made of alternating P3HT (donor) and **SWCNT-PhTh** (acceptor) thin layers. In this way, we are able to obtain a high control on the organization and on the interface between the different components.[60, 61]

In particular, we prepared a (3+3)x2 MHJ structure. This structure consists of three consecutive layers of **SWCNT-PhTh** derivatised in batch deposited onto three layers of P3HT and repeated twice, for a total of twelve layers. In this way, we ensured homogeneous domains for each component, although the donor/acceptor interfacial area is limited. In order to explore a wider donor-acceptor interaction range, in addition to the as-prepared MHJ samples (Fig. 7a) the fluorescence quenching measurements were performed on annealed MHJs (Fig. 7b) and in spin coated thin films, that are both BHJs with larger interface area (Fig. 7c).

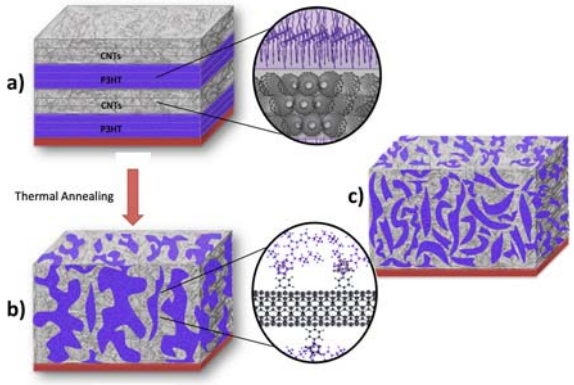

Fig. 7 Schematic representation of three different P3HT:SWCNT heterojunctions: a) multi-planar heterojunction, b) bulk heterojunction obtained by thermal annealing of the multi-planar heterojunction, c) bulk heterojunction obtained by spin-coating

Spin coating was performed by a solution of P3HT and **SWCNT-PhTh** in chlorobenzene.

Thanks to the approach in Fig. 7b, a modulation of the characteristics of the heterojunction architectures (i.e., interfacial

area and percolation pathways) may be achieved simply by changing the dynamic parameters (i.e., time and thermal energy).[60] Arguably, the thermal annealing of a MHJ may lead to an intermediate architecture providing high interfacial surface, and thus a high probability for exciton dissociation, and extended percolation channels for charge transport.[60]

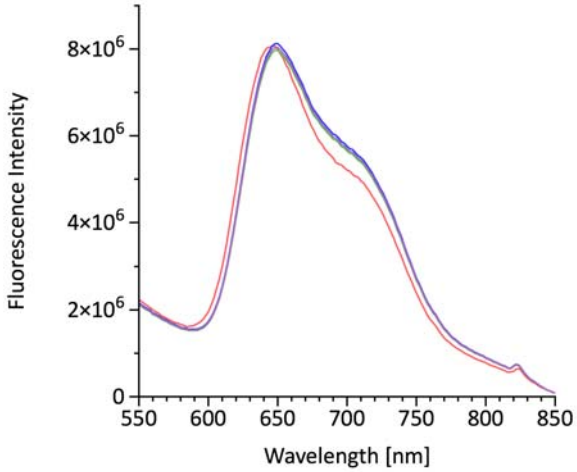

Fig. 8 Fluorescence spectra of pristine P3HT (red line), MHJ (blue line), annealed MHJ (green line) and BHJ by spin-coating (purple line) with **SWCNT-PhTh** derivatised in batch.

Fig. 8 shows fluorescence spectra of the pristine P3HT and of three different structures: MHJ, MHJ annealed at 130 °C for 5 minutes and BHJ obtained by spin-coating the soluble extract of **SWCNT-PhTh** derivatised in batch. In this case, it is evident that the presence of nanotubes does not induce any changes in the luminescence of P3HT, irrespective of the heterostructure considered. Arguably, this is an evidence of the lack of electronic interaction between P3HT and the carbon nanotubes functionalized in batch conditions.

On the other hand, by performing the experiment with **SWCNT-PhTh** derivatised in flow we observed an appreciable P3HT fluorescence quenching in all the architectures (MHJ, spin coated BHJ and annealed MHJ) (Fig. 9) spanning from 47% to 70% for the MHJ and spin coated BHJ, respectively. This shows that there is a significant interaction between P3HT and **SWCNT-PhTh** functionalized in flow conditions with all the heterojunction architectures. Nevertheless, the increased interface area of the BHJ architectures results in a higher fluorescence quenching. Moreover, when we annealed the MHJ (130 °C for 5 minutes) we obtained a quenching value (~70%) similar to that of the spin-coated BHJ. Also by changing the annealing time (130 °C for 15 sec) we were able to modulate the fluorescence quenching more likely because of a change of the interfacial area indicating that P3HT and **SWCNT-PhTh** functionalized in flow are able to undergo a controlled inter-diffusion.

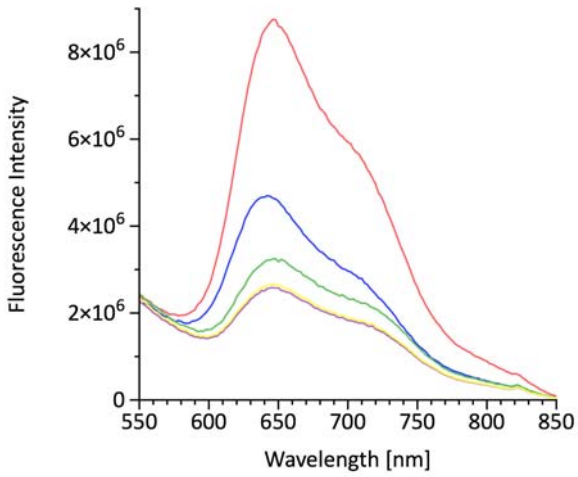

Fig. 9 Fluorescence spectra of pristine P3HT (red line), MHJ (blue line), annealed MHJ for 15'' (green line), annealed MHJ for 5' (purple line) and BHJ by spin-coating (yellow line) with **SWCNT-PhTh** derivatised in flow.

Conclusions

We have reported an insight into the use of functionalized SWCNTs for optoelectronic applications by forming heterojunction devices with P3HT. In particular, we have provided evidence that an excessive modification of the SWCNT surface, due to the high number of carbon atoms converted from sp^2 to sp^3 after the functionalization, results in the loss of the electronic and thermal properties of pristine nanotubes. In agreement with our previous study, fluorescence quenching measurements of **SWCNT-PhTh**/P3HT blends show that an uncontrolled functionalization shields the surface of SWCNTs thus preventing it from interacting with P3HT. On the other hand, the use of non-conventional methods for the controlled functionalization of SWCNTs has allowed us to prepare a **SWCNT-PhTh** derivative with a good trade-off between solubility, and thus processability, and preservation of SWCNT properties required for an electronic interaction with P3HT.

Acknowledgements

This work was supported by MIUR (grants FIRB-Futuro in Ricerca RBFR08DUX6, FIRB RBAP11C58Y, PRIN 20104XET32) and Regione del Veneto (SMUPR n. 4148, Polo di Ricerca nel settore fotovoltaico).

Notes and references

[a] *Università di Padova, Dipartimento di Scienze Chimiche, via Marzolo, 1 35131, Padova, Italy. E-mail: enzo.menna@unipd.it; Tel: + 39 0498275660*

[b] *Università di Palermo, Dipartimento di Fisica e Chimica, V.le delle Scienze, Parco d'Orleans II, 90128, Palermo, Italy. Email: bruno.pignataro@unipa.it; Tel: +39 09123897983*

[c] *Consiglio Nazionale delle Ricerche, Istituto di Biostrutture e Bioimmagini (IBB-CNR), Via Mezzocannone 16, I-80136, Napoli, Italy.*

† Electronic Supplementary Information (ESI) available: [details of any supplementary information available should be included here]. See DOI: 10.1039/b000000x/

‡ Footnotes should appear here. These might include comments relevant to but not central to the matter under discussion, limited experimental and spectral data, and crystallographic data.

1. S. Cataldo, P. Salice, E. Menna and B. Pignataro, *Energy Environ. Sci.*, 2012, **5**, 5919-5940.
2. L. Wang, H. Liu, R. M. Konik, J. A. Misewich and S. S. Wong, *Chem. Soc. Rev.*, 2013, **42**, 8134-8156.
3. D. Liming, H. Pingang and L. Sinan, *Nanotechnology*, 2003.
4. D. Jariwala, V. K. Sangwan, L. J. Lauhon, T. J. Marks and M. C. Hersam, *Chem. Soc. Rev.*, 2013, **42**, 2824-2860.
5. V. C. Tung, J.-H. Huang, J. Kim, A. J. Smith, C.-W. Chu and J. Huang, *Energy Environ. Sci.*, 2012, **5**, 7810-7818.
6. M.-Y. Wu, R. M. Jacobberger and M. S. Arnold, *J. Appl. Phys.*, 2013, **113**, 204504-204504-204515.
7. D. D. Tune and J. G. Shapter, *Energy Environ. Sci.*, 2013, **6**, 2572-2577.
8. M.-H. Ham, G. L. C. Paulus, C. Y. Lee, C. Song, K. Kalantar-zadeh, W. Choi, J.-H. Han and M. S. Strano, *ACS Nano*, 2010, **4**, 6251-6259.
9. D. J. Bindl, N. S. Safron and M. S. Arnold, *ACS Nano*, 2010, **4**, 5657-5664.
10. H. Kataura, Y. Kumazawa, Y. Maniwa, I. Umezu, S. Suzuki, Y. Ohtsuka and Y. Achiba, *Synth. Met.*, 1999, **103**, 2555-2558.
11. H. Liu, T. Tanaka, Y. Urabe and H. Kataura, *Nano Lett.*, 2013, **13**, 1996-2003.
12. T. Kobayashi, Z. Nie, J. Du, K. Okamura, H. Kataura, Y. Sakakibara and Y. Miyata, *Phys. Rev. B*, 2013, **88**, 035424.
13. D. W. Schaefer and R. S. Justice, *Macromolecules*, 2007, **40**, 8501-8517.
14. C. Bounioux, E. A. Katz and R. Yerushalmi – Rozen, *Polym. Adv. Technol.*, 2012, **23**, 1129-1140.
15. J. Gao, R. Annema and M. A. Loi, *Eur. Phys. J. B*, 2012, **85**, 1-5.
16. W. Gomulya, J. Gao and M. A. Loi, *Eur. Phys. J. B*, 2013, **86**, 1-13.
17. I. Musa, M. Baxendale, G. A. J. Amaratunga and W. Eccleston, *Synth. Met.*, 1999, **102**, 1250-1250.
18. E. Kymakis, I. Alexandou and G. A. J. Amaratunga, *Synth. Met.*, 2002, **127**, 59-62.
19. E. Kymakis and G. Amaratunga, *Appl. Phys. Lett.*, 2002, **80**, 112-114.
20. E. Kymakis, I. Alexandrou and G. A. J. Amaratunga, *J. Appl. Phys.*, 2003, **93**, 1764-1768.
21. E. Kymakis and G. A. J. Amaratunga, *Sol. Energy Mater.*, 2003, **80**, 465-472.
22. E. Kymakis and G. Amaratunga, *Rev. Adv. Mater. Sci.*, 2005, **10**, 300-305.
23. S. Berson, R. de Bettignies, S. Bailly, S. Guillerez and B. Jousselme, *Adv. Funct. Mater.*, 2007, **17**, 3363-3370.
24. S. D. Stranks, S. N. Habisreutinger, B. Dirks and R. J. Nicholas, *Adv. Mater.*, 2013, **25**, 4365-4371.
25. S. Niyogi, M. A. Hamon, H. Hu, B. Zhao, P. Bhowmik, R. Sen, M. E. Itkis and R. C. Haddon, *Acc. Chem. Res.*, 2002, **35**, 1105-1113.
26. P. Salice, D. Fenaroli, C. C. De Filippo, E. Menna, G. Gasparini and M. Maggini, *Chim. Oggi-Chem. Today*, 2012, **30**, 37-39.
27. E. Menna, F. Della Negra, M. Dalla Fontana and M. Meneghetti, *Phys. Rev. B*, 2003, **68**, 193412.
28. M. D'Este, M. D. Nardi and E. Menna, *Eur. J. Org. Chem.*, 2006, **2006**, 2517-2522.
29. J. Chen, M. A. Hamon, H. Hu, Y. Chen, A. M. Rao, P. C. Eklund and R. C. Haddon, *Science*, 1998, **282**, 95-98.
30. B. Gebhardt, R. Graupner, F. Hauke and A. Hirsch, *Eur. J. Org. Chem.*, 2010, **2010**, 1494-1501.
31. P. Salice, E. Rossi, A. Pace, P. Maity, T. Carofiglio, E. Menna and M. Maggini, *J. Flow Chem.*, 2014, **4**, 79-85.
32. J. L. Bahr and J. M. Tour, *Chem. Mater.*, 2001, **13**, 3823-3824.
33. L. Rodríguez-Pérez, R. García, M. Á. Herranz and N. Martín, *Chem.-Eur. J.*, 2014, **20**, 7177-7177.
34. C. A. Dyke and J. M. Tour, *J. Phys. Chem. A*, 2004, **108**, 11151-11159.
35. J. L. Hudson, M. J. Casavant and J. M. Tour, *J. Am. Chem. Soc.*, 2004, **126**, 11158-11159.
36. J. N. Coleman, *Adv. Funct. Mater.*, 2009, **19**, 3680-3695.
37. S. D. Bergin, Z. Sun, D. Rickard, P. V. Streich, J. P. Hamilton and J. N. Coleman, *ACS Nano*, 2009, **3**, 2340-2350.
38. P. Salice, P. Maity, E. Rossi, T. Carofiglio, E. Menna and M. Maggini, *Chem. Commun.*, 2011, **47**, 9092-9094.
39. Z. Salmi, S. Gam-Derouich, S. Mahouche-Chergui, M. Turmine and M. Chehimi, *Chem. Pap.*, 2012, **66**, 369-391.
40. M. M. Chehimi, *Aryl Diazonium Salts*, Wiley-VCH, 2012.
41. P. Salice, E. Fabris, C. Sartorio, D. Fenaroli, V. Figà, M. P. Casaletto, S. Cataldo, B. Pignataro and E. Menna, *Carbon*, 2014, **74**, 73-82.
42. G. E. Collis, A. K. Burrell, S. M. Scott and D. L. Officer, *J. Org. Chem.*, 2003, **68**, 8974-8983.
43. P. Hrobárik, V. Hrobáriková, I. Sigmundová, P. Zahradník, M. Fakis, I. Polyzos and P. Persephonis, *J. Org. Chem.*, 2011, **76**, 8726-8736.
44. D. Bouilly, J. Cabana, F. o. Meunier, M. Desjardins-Carrière, F. o. Lapointe, P. Gagnon, F. L. Larouche, E. Adam, M. Paillet and R. Martel, *ACS Nano*, 2011, null-null.
45. J. Bahr, E. Mickelson, M. Bronikowski, R. Smalley and J. Tour, *Chem. Commun.*, 2001, **2001**, 193-194.
46. J. Bahr and J. Tour, *J. Mater. Chem.*, 2002, **12**, 1952-1958.
47. E. Stendardo, F. Avila Ferrer, F. Santoro and R. Improta, *J. Chem. Theory Comput.*, 2012, **8**, 4483-4493.
48. J. Tomasi, B. Mennucci and R. Cammi, *Chem. Rev.*, 2005, **105**, 2999-3094.
49. M. J. Frisch, G. W. Trucks, H. B. Schlegel, G. E. Scuseria, M. A. Robb, J. R. Cheeseman, G. Scalmani, V. Barone, B. Mennucci, G. A. Petersson, H. Nakatsuji, M. Caricato, X. Li, H. P. Hratchian, A. F. Izmaylov, J. Bloino, G. Zheng, J. L. Sonnenberg, M. Hada, M. Ehara, K. Toyota, R. Fukuda, J. Hasegawa, M. Ishida, T. Nakajima, Y. Honda, O. Kitao, H. Nakai, T. Vreven, J. A. Montgomery, Jr., J. E. Peralta, F. Ogliaro, M. Bearpark, J. J. Heyd, E. Brothers, K. N. Kudin, V. N. Staroverov, R. Kobayashi, J. Normand, K. Raghavachari, A. Rendell, J. C. Burant, S. S. Iyengar, J. Tomasi, M. Cossi, N. Rega, J. M. Millam, M. Klene, J. E. Knox, J. B. Cross, V. Bakken, C. Adamo, J. Jaramillo, R. Gomperts, R. E. Stratmann, O. Yazyev, A. J. Austin, R. Cammi, C. Pomelli, J. W. Ochterski, R. L. Martin, K. Morokuma, V. G. Zakrzewski, G. A. Voth, P. Salvador, J. J. Dannenberg, S. Dapprich, A. D. Daniels, Ö. Farkas, J. B. Foresman, J. V. Ortiz, J. Cioslowski and D. J. Fox, Gaussian Inc., Wallingford CT, 2009.

50. M. M. Stylianakis, J. A. Mikroyannidis and E. Kymakis, *Sol. Energy Mater.*, 2010, **94**, 267-274.
51. A. F. Nogueira, B. S. Lomba, M. A. Soto-Oviedo, C. R. D. Correia, P. Corio, C. A. Furtado and I. A. Hümmelgen, *J. Phys. Chem. C*, 2007, **111**, 18431-18438.
52. S. M. Bachilo, M. S. Strano, C. Kittrell, R. H. Hauge, R. E. Smalley and R. B. Weisman, *Science*, 2002, **298**, 2361-2366.
53. M. J. O'Connell, S. M. Bachilo, C. B. Huffman, V. C. Moore, M. S. Strano, E. H. Haroz, K. L. Rialon, P. J. Boul, W. H. Noon, C. Kittrell, J. Ma, R. H. Hauge, R. B. Weisman and R. E. Smalley, *Science*, 2002, **297**, 593-596.
54. C. A. Dyke and J. M. Tour, *Nano Lett.*, 2003, **3**, 1215-1218.
55. The concentrations of the solution of SWCNT-PhTh were calculated contextually to the TGA measurements. Briefly, 500 μL of each solution was drop casted and annealed at 120°C on a platinum crubicle for TGA analysis. The weight measured at the beginning of the TGA analysis was used to calculate the concentration of SWCNT-PhTh in solution.
56. M. S. Dresselhaus, A. Jorio, M. Hofmann, G. Dresselhaus and R. Saito, *Nano Lett.*, 2010, **10**, 751-758.
57. M. S. Dresselhaus, A. Jorio, A. G. Souza Filho and R. Saito, *Philos. Trans. R. Soc. London, A*, 2010, **368**, 5355-5377.
58. G. Bottari, G. de la Torre, D. M. Guldi and T. Torres, *Chem. Rev.*, 2010, **110**, 6768-6816.
59. A. Ahmad, T. Kurkina, K. Kern and K. Balasubramanian, *ChemPhysChem*, 2009, **10**, 2251-2255.
60. S. Cataldo, C. Sartorio, F. Giannazzo, A. Scandurra and B. Pignataro, *Nanoscale*, 2014, **6**, 3566-3575.
61. S. Cataldo and B. Pignataro, *Materials*, 2013, **6**, 1159-1190.

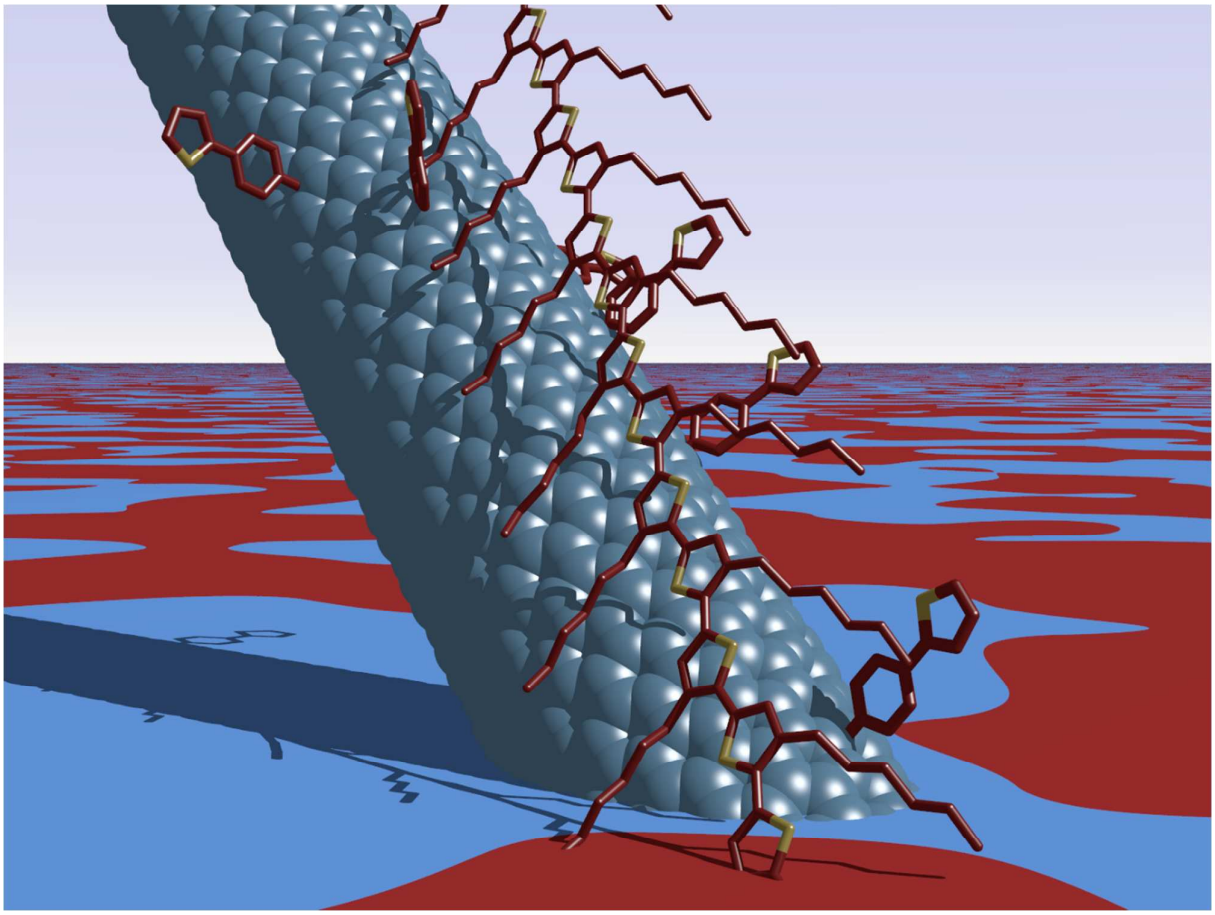

Controlled functionalization of single wall carbon nanotubes through flow chemistry: a mean to improve processability while preserving electronic interaction with a semiconducting polymer in thin film heterojunctions.